Evolutionary topology optimization of continuum structures with smooth boundary representation

Daicong Da[a,b], Liang Xia[c], Guangyao Li[a,b*], Xiaodong Huang[a,d*]

[a] State Key Laboratory of Advanced Design and Manufacturing for Vehicle Body, Hunan University, Changsha, PR China

[b] Joint Center for Intelligent New Energy Vehicle, Shanghai, PR China

[c] State Key laboratory of Digital Manufacturing Equipment and Technology, Huazhong University of Science and Technology, Wuhan, China

[d]Faculty of Science, Engineering and Technology, Swinburne University of Technology, Hawthorn, Melbourne, VIC 3122, Australia

* Corresponding author. Email: xhuang@swin.edu.au (Xiaodong Huang); gyli@hnu.edu.cn (Guangyao Li)

Abstract: This paper develops an extended bi-directional evolutionary structural optimization (BESO) method for topology optimization of continuum structures with smoothed boundary representation. In contrast to conventional zigzag BESO designs and removal/addition of elements, the newly proposed evolutionary topology optimization (ETO) method, determines implicitly the smooth structural topology by a level-set function (LSF) constructed by nodal sensitivity numbers. The projection relationship between the design model and the finite element analysis (FEA) model is established. The analysis of the design model is replaced by the FEA model with various elemental volume fractions, which are determined by the auxiliary LSF. The introduction of sensitivity LSF results in intermediate volume elements along the solid-void interface of the FEA model, thus contributing to the better convergence of the optimized topology for the design model. The effectiveness and robustness of the proposed method are verified by a series of 2D and 3D topology optimization design problems including compliance minimization and natural frequency maximization. It has been shown that the developed ETO method is capable of generating a clear and smooth boundary representation; meanwhile the resultant designs are less dependent on the initial guess design and the finite element mesh resolution.

Keywords: Topology optimization; Evolutionary topology optimization (ETO); Level-set function; Smooth boundary representation

1. Introduction

Over the past decades, topology optimization has undergone a tremendous development since the seminal paper by Bensøe and Kikuchi [1]. The key merit of topology optimization over conventional size and shape optimization is that the former can provide more design freedom, consequently leading to the creation of novel and highly efficient designs. So far, various topology optimization methods have been proposed, e.g., density-based method [2-4], evolutionary procedures [5-6], level-set method (LSM) [7-9], hybrid cellular automaton [10] and phase field method [11]. All of these methods are based on finite element analysis (FEA) where the design domain is discretized into a number of finite elements. With such a setting, the optimization procedure is then to determine which points of the design domain should be full of material (solid element) and the others are void (or soft elements). According to the update algorithm, these methods can be categorized in general into two groups: density variation and shape/boundary variation. So far, topology optimization technique has already become an effective tool for both academic researches and engineering applications. A general review on various methods and their applications has been presented by Deaton and Grandhi [12]. Regarding their strengths, weaknesses, similarities and dissimilarities, a critical review and comparison on different approaches has also been reviewed by Sigmund and Maute [13].

LSM is a typical shape/boundary variation approach whilst maintains the capability of topological change. It describes the structural topology implicitly by the iso-contours of a level-set function. By LSM, a fixed rectilinear spatial grid and a finite element mesh of a given design domain are constructed separately, which allows the separation of the topological description and the physical model. With the merits of the flexibility in handling complex topological changes and the smoothness of boundary representation, LSM has been successfully applied to an increasing variety of design problems, involving e.g., multi-phase materials, shell structures, geometric nonlinearities, stress minimization and contact problem [14-18]. However, the resultant designs by LSM are highly dependent on the initial guess design and the adopted regularization techniques. Another important challenge of LSM-based topology optimization is the convergence issue observed by the apparent oscillations in the optimization process. The reader is referred to the comprehensive review by van Dijk et al. [19] for more theoretical details of different LSMs for structural topology

optimization.

Density-based methods are the most commonly used topology optimization approaches, such as the popular solid with isotropic material with penalization (SIMP) method. The SIMP method uses continuous design variables for topology optimization, which can be interpreted as material pseudo densities [2-3, 20]. The physical justification of SIMP was provided by Bendsøe and Sigmund [21]. A popular 99-line topology optimization Matlab code using the SIMP method was developed in Sigmund [22] for education purposes. As a successor of the 99-line code, a more efficient 88-line Matlab code was also provided by Andreassen et al. [23] with high computational efficiency and alternative filter implements. More details including theory, numerical methods and applications on the SIMP method can be found in [4].

As another important branch of topology optimization, evolutionary structural optimization (ESO) [5-6, 24] and its later version bi-directional ESO (BESO) [25] have shown promising performance when applying to a wide range of structural design problems. ESO-type methods use a simple heuristic scheme to evolve the structural topology towards an optimum by gradual removing redundant or inefficient materials. The BESO method allows not only material removal, but also material addition, showing efficient and reliable performance in various design problems [26-34]. The early development of ESO-type methods was summarized by Xie and Steven [35]. The development of the BESO method and its various applications up to year 2010 can been founded in [36]. A comprehensive review on the BESO method for advanced design of structures and materials was recently presented by Xia et al. [37].

Note that by the density-based approaches, either continuous (SIMP) or discrete (ESO/BESO), the structural topology is determined via element-wisely defined pseudo densities, resulting in a zigzag boundary representation. So it is of great significance in practice to achieve topology designs with refined or smooth boundary representation. In this context, the LSM [7-9, 14-19, 38] allows analyzing continuously moving material interfaces and ensure a smooth topological boundary. Taking the advantages of element-based topology optimization and an elegant treatment of boundary smoothness, the fix-grid (FG) FEA framework [39] had been applied to topology optimization based on ESO [40-41] and BESO [42]. In their wok, a B-spline representation of boundary was adopted for shape or topology optimization and the design variables of FG ESO/BESO were still based on elements. Assuming that the design domain is full of fine grid points (much more than elements), design variables

of topology optimization should be ideally those points rather than elements so that the resulting topology can be accurately expressed by smooth boundary.

This work develops an extended BESO method for topology optimization of continuum structures with smooth boundary representation. The design model and the FEA model are established for topology representation and numerical calculation, respectively. In contrast to conventional zigzag BESO designs and removal/addition of elements, the newly proposed evolutionary topology optimization (ETO) method, determines implicitly the smooth structural topology using a constructed level-set function (LSF) based on sensitivity analysis. The results will save the cost involving the post-processing of optimized topology. The remainder of this paper is organized as follows: Section 2 presents the proposed ETO design framework with the relationship between the FEA and the design models as well as the construction of sensitivity LSF. Several typical topology optimization problems including compliance minimization and natural frequency maximization are formulated. Section 3 gives numerical implementations of the developed ETO procedure. Section 4 presents a series of numerical validations of the ETO method. Section 5 draws the conclusion. A Matlab code using the ETO method for compliance minimization design is provided in Appendix.

2. ETO method framework

2.1 Design and FEA models

The conventional BESO method optimizes a structure by gradually removing and adding finite elements upon their sensitivity numbers. That is to say that the element itself is treated as a design variable and the structural topology is typically described via element-wise constant, i.e., element pseudo density. This implementation results in designs with zigzag boundaries, especially when a coarse FE mesh is used. In this work, we propose an extended BESO method, namely evolutionary topology optimization (ETO), aiming at obtaining optimized structures with smooth boundary. Since topology optimization requires to update the structural shape iteratively, FEA of a smooth structure can be ideally performed by using the re-meshing technique after each design iteration but computationally extreme expensive. The simpler and efficient Area-fraction (or volume-fraction in three dimensional cases) weighted Fixed Grid (AFG)

method, which has been widely used by spline and level-set based optimization methods [38, 39, 41, 43-46], is adopted in the present work.

In the proposed ETO method, we separate the design model from the FEA model and establish the project relationship between two models as shown in Fig. 1. The design model represents the smooth structural topology, which will be determined by the constructed LSF in the later section. When the design model projects onto the background mesh with the fixed grid, the volume fraction of each element, V_i^{f}, can be easily calculated and three categories of elements are generated: void elements with $V_i^{\mathrm{f}} = 0$; solid elements with $V_i^{\mathrm{f}} = 1$ and boundary elements with $0 < V_i^{\mathrm{f}} < 1$. FEA will be conducted on the fixed-grid model and material properties of elements will be defined with

$$\rho_i\left(V_i^f\right) = \left(1 - V_i^{\mathrm{f}}\right)\rho_{min} + V_i^{\mathrm{f}}\rho_0$$
$$E_i\left(V_i^f\right) = \left(1 - V_i^{\mathrm{f}}\right)E_{min} + V_i^{\mathrm{f}}E_0 \quad (1)$$

where ρ and E are the density and Young's modulus. The subscripts 0 and *min* denote the solid and void materials, respectively. ρ_{min} and E_{min} are small values in order to avoid the singularity of mass and stiffness matrices. Thus, the analysis of the design model can be replaced by the fixed-grid FEA model so as to avoid re-meshing after each iteration.

2.2 Problem statements and sensitivity analysis

2.2.1 Problem statements

One typical topology optimization problem is structural compliance minimization (i.e., stiffness maximization) subject to a volume constraint based on the design model, which is firstly considered here as

$$\begin{aligned} &min : C \\ &\text{subject to} : V = V^* \\ &\qquad\quad : x_o = 0 \text{ or } 1 \end{aligned} \quad (2)$$

where C is the structural compliance, V and V^* and are the structural volume and its constraint value. x_o is a binary variable and o=o(x, y) denotes an arbitrary point within the design domain. $x_o = 1$ means that the point is full of solid and $x_o = 0$ means void.

According to the relationship between the design model and the FEA model as

shown in Fig. 1, the structural volume of the design model, V can be expressed by

$$V = \sum_{i=1}^{N} V_i^{\mathrm{f}} V_i \text{ and } 0 \le V_i^{\mathrm{f}} \le 1 \quad (3)$$

where V_i denotes the volume of the ith element volume and N is the total element number in the FEA model. It is assumed that an element in the FEA model corresponds to a number of gird points (40×40 in 2D cases in this paper) in the design model. The element would be a solid element, $V_i^{\mathrm{f}} = 1$, when all corresponding grid points, x_o, in the design model are solid, or a void element, $V_i^{\mathrm{f}} = 0$, when all points are void. Otherwise, the element would be a boundary element, $0 < V_i^{\mathrm{f}} < 1$, which contains both solid and void grid points in the design model. Thus, the mechanical properties of elements in the FEA model with regard to different volume fractions are calculated according to Eqns. (1) and (2).

The compliance of the design model should be equal to that of the FEA model, which can be expressed by.

$$C = \mathbf{F}^T \mathbf{U} \quad (4)$$

Where $\mathbf{F}$ and $\mathbf{U}$ are the applied load and displacement vectors, respectively. The equilibrium equation of the FEA model is

$$\mathbf{F} = \mathbf{K}\mathbf{U} \quad (5)$$

where $\mathbf{K}$ is the global stiffness matrix.

Frequency optimization is of great importance in many engineering field, e.g., aerospace and automotive industries. The dynamic behavior of a structure can be represented by the following general eigenvalue problem

$$\left(\mathbf{K} - \omega_j^2 \mathbf{M}\right)\mathbf{u}^{(j)} = 0 \quad (6)$$

where $\mathbf{M}$ is the global mass matrix, ω_j is the j-th natural frequency and $\mathbf{u}^{(j)}$ is the eigenvector corresponding to ω_j. ω_j and $\mathbf{u}^{(j)}$ are related to each other by the following Rayleigh quotient

$$\omega_j^2 = \frac{(\mathbf{u}^{(j)})^T \mathbf{K}\mathbf{u}^{(j)}}{(\mathbf{u}^{(j)})^T \mathbf{M}\mathbf{u}^{(j)}} \quad (7)$$

The topology optimization for maximizing a natural frequency can be mathematically defined based on the design model as

$$\begin{aligned} &\max : \ \omega_j \\ &\text{subject to} : V = V^* \\ &\qquad\qquad : x_0 = 0 \text{ or } 1 \end{aligned} \quad (8)$$

where ω_j of the design model is equal to that of the FEA model calculated from Eqn. (7).

2.2.2 Sensitivity analysis

Ideally, sensitivity analysis should be conducted based on the design model against the design variable, x_o. However, the design model does not involve in analysis and therefore sensitivity analysis is conducted based on the FEA model instead. Although elemental volume fractions, V_i^{f}, are used in the FEA model for analyzing the design model, they can not be used as the design variables for topology optimization. The reason is that V_i^{f} does not be freely varied within the design domain and the intermediate volume fraction, $0 < V_i^{\mathrm{f}} < 1$ is only allowed on the boundary of the structural topology. In other words, any solution with two or more layers of intermediate elements along boundary should be excluded from the solution domain. Therefore, to achieve a solid/void design for continuum structures, an artificial design variable for each element within the FEA model, x_i, is introduced and the well-known SIMP model [2-4] is used for the material interpolation scheme as

$$E(x_i) = x_i^p E_0 \tag{9}$$

where p is the penalty factor. p>1 is the necessary condition to make sure the existence of 0/1 solution [4] and p = 3 is used in this paper. It should be noted that the material interpolation scheme in Eqn. (9) is used for topology optimization of the FEA model. But Eqn.(1) is adopted so that the calculation of the design model can be accurately replaced by the FEA model.

With the above material interpolation scheme, the sensitivity of structural compliance on the design variable, x_i, can be derived through the adjoint method [4], as

$$\frac{\partial C}{\partial x_i} = -p x_i^{p-1} \mathbf{u}_i^T \mathbf{k}_i^0 \mathbf{u}_i \tag{10}$$

where $\mathbf{u}_i$ is the nodal displacement vector of the o-th element and $\mathbf{k}_i^0$ denotes the stiffness matrix of the solid element. The sensitivity number for compliance minimization is defined as its sensitivity multiplied with a constant, $-1/p$, as [36]

$$\alpha_i = -\frac{1}{p}\frac{\partial C}{\partial x_i} = x_i^{p-1} \mathbf{u}_i^T \mathbf{k}_i^0 \mathbf{u}_i \tag{11}$$

When the *i*th-element is solid or void, the sensitivity number of the *i*th element can be explicitly written as

$$\alpha_i = \begin{cases} \mathbf{u}_i^T \mathbf{k}_i^0 \mathbf{u}_i & \text{when } x_i = 1 \\ x_{min}^{p-1} \mathbf{u}_i^T \mathbf{k}_i^0 \mathbf{u}_i & \text{when } x_i = x_{min} \end{cases} \tag{12}$$

Since elements in the FEA model can be viewed as solid with V_i^{f} and void with (1-V_i^{f}), the sensitivity number for the *i*th element can be approximately estimated with

$$\alpha_i = \left[x_{min}^{p-1}\left(1 - V_i^{\mathrm{f}}\right) + V_i^{\mathrm{f}}\right] \mathbf{u}_i^T \mathbf{k}_i^0 \mathbf{u}_i \tag{13}$$

As for frequency optimization, it also needs the material interpolation scheme for density as

$$\rho(x_i) = x_i \rho_0 \tag{14}$$

Compared with the extensive research on stiffness optimization, topology optimization for natural frequency is more challenging due to the possible localized modes [27, 47]. To avoid artificial localized modes, we can keep the ratio between mass and stiffness constants of void elements to be equal that of solid elements as [27], i.e. $\rho_{min}/E_{min} = \rho_0/E_0$. Using the adjoint method, the element sensitivity of natural frequency on the design variable, x_i, defined as [27]

$$\frac{\partial \omega_j}{\partial x_i} = \frac{1}{2\omega_j} \mathbf{u}_i^{(j)T} \left[\frac{1 - x_{min}}{1 - x_{min}^p} p x_i^{p-1} \mathbf{k}_i^0 - \omega_j^2 \mathbf{m}_i^0\right] \mathbf{u}_i^{(j)} \tag{15}$$

where $\mathbf{m}_i^0$ is the mass matrix of the solid element and therefore the sensitivity numbers for solid and void elements are expressed explicitly as

$$\alpha_i = \frac{1}{p}\frac{\partial \omega_j}{\partial x_i} = \begin{cases} \frac{1}{2\omega_j} \mathbf{u}_i^{(j)T} \left[\frac{1 - x_{min}}{1 - x_{min}^p} \mathbf{k}_i^0 - \frac{\omega_j^2}{p} \mathbf{m}_i^0\right] \mathbf{u}_i^{(j)} & \text{when } x_i = 1 \\ \frac{1}{2\omega_j} \mathbf{u}_i^{(j)T} \left[\frac{1 - x_{min}}{1 - x_{min}^p} x_{min}^{p-1} \mathbf{k}_i^0 - \frac{\omega_j^2}{p} \mathbf{m}_i^0\right] \mathbf{u}_i^{(j)} & \text{when } x_i = x_{min} \end{cases} \tag{16}$$

Thus, the sensitivity number for the *i*th element with volume fraction, V_i^{f}, is

$$\alpha_i = \frac{1}{2\omega_j} \mathbf{u}_i^{(j)T} \left\{\frac{1 - x_{min}}{1 - x_{min}^p}\left[V_i^{\mathrm{f}} + x_{min}^{p-1}\left(1 - V_i^{\mathrm{f}}\right)\right] \mathbf{k}_i^0 - \frac{\omega_j^2}{p} \mathbf{m}_i^0\right\} \mathbf{u}_i^{(j)} \tag{17}$$

2.3 Nodal sensitivity numbers and level set function

In order to determine the smooth topology of the design model, we will construct the level-set function based on the nodal sensitivity numbers of the FEA model. It is well known that 0/1 solution for the topology optimization problem defined in Eqn. (2) does not exist. The reason is that the introduction of more holes, without changing the structural volume, will generally increase the efficiency of a given structure [4]. In the limit of this process, one fails to obtain a 0/1 solution unless a specified size constraint is specified. However, it is extremely challenging to impose an exact size constraint in

the topology optimization algorithm [48]. A most convenient and popular way is to use the heuristic filter [49], which works as a low-pass filter that eliminates structural components below a certain length-scale in the optimal design based on an image-processing technique. Here, we adopt the filter scheme, which transfers sensitivity numbers from elements to nodes as

$$\hat{\alpha}_j = \frac{\sum_{i=1}^{M} w_{ij}\alpha_i}{\sum_{i=1}^{M} w_{ij}} \tag{18}$$

where $\hat{\alpha}_j$ denote the sensitivity number at the *j*th node. w_{ij} is a linear weight factor with

$$\omega_{ij} = \max\left(0, r_{min} - r(i,j)\right) \tag{19}$$

where r_{min} is the prescribed filter radius and $r(i,j)$ denotes the distance between element *i* and node *j*.

To further improve the convergence of the objective function, the nodal sensitivity is further modified with its sensitivity history as [25]

$$(\tilde{\alpha}_j)_l = \frac{\left[(\hat{\alpha}_j)_l + (\tilde{\alpha}_j)_{l-1}\right]}{2} \tag{20}$$

where the subscript l denotes the current iteration number. Thus, the updated sensitivity number includes all sensitivity information in the previous iterations.

Next, we will develop the LSF for the design model. Different from the traditional LSF governed by the Hamilton-Jacobi equation [7-9, 38, 41, 43-46], the current LSF is constructed based on the nodal sensitivity numbers. According to the project relationship as shown in Fig. 1, the LSF value of the design model is equal to the nodal sensitivity number of the FEA model, $\phi_j = \tilde{\alpha}_j$. For an arbitrary point, $o(\xi_o, \eta_o)$, within, e.g., rectangular element *i*, the LSF value can be linearly expressed by

$$\phi(o) = \sum_{j=1}^{4} N_j(o)\phi_i^j \tag{21}$$

where ϕ_i^j denote the LSF value at the *j*th node of element *i*. ξ_o and η_o are non-dimensional coordinates of point o in the natural coordinate system as shown in Fig. 2. $N_j(o)$ denotes the standard interpolation function. Under 2D cases, it is expressed by

$$N_j(o) = \frac{1}{4}((1 + \xi_o\xi_j) + (1 + \eta_o\eta_j)) \tag{22}$$

where ξ_j and η_j are local coordinates of the *j*th node. The construction of the

sensitivity-based LSF can be equally extended for 3D cases.

2.4 Update of structural topology

With the constructed nodal sensitivity-based LSF $\phi(o)$, the LSM defines the design domain (D) of the design model as solid regions (Ω), void regions ($D\backslash\Omega$) and boundaries (Γ) by setting the level-set value as shown in Fig. 3.

$$\begin{cases} \phi(o) > S \;\Leftrightarrow\; o \in \Omega \\ \phi(o) = S \;\Leftrightarrow\; o \in \Gamma \\ \phi(o) < S \;\Leftrightarrow\; o \in D\backslash\Omega \end{cases} \tag{23}$$

where S is the level-set value which is calculated iteratively by using the bi-section method so as to satisfy the target material volume at each iteration. Different from the topology derived by the normal velocity of the boundary in the traditional LSM [38, 39, 41, 43-46], the update of topology in the proposed method is realized by setting the level-set value in each iteration.

To calculate the level-set value, the target volume of the design model for the current iteration, V_l, needs to be determined first. Since the constraint volume V^* could be larger, smaller or equal to the volume of the initial guess design, the target volume in each iteration may decrease, increase step by step, or keep constant so as to finally satisfy the volume constraint, V^*. Given the volume of the last iteration, V_{l-1}, the target volume of the current iteration, V_l, can be calculated according to

$$V_l = \begin{cases} \max(V_{l-1}(1-ER), V^*) & \text{if } V_{l-1} \geq V^* \\ \min(V_{l-1}(1+ER), V^*) & \text{if } V_{l-1} < V^* \end{cases} \tag{24}$$

where ER is an evolution rate, e.g. 2% in this paper. Thus, the volume of the design model gradually evolves to its constraint value, V^*, in the framework of the evolutionary optimization procedure.

Since the fixed-grid mesh is used in the FEA model, it has three different types of elements, i.e., solid, void and boundary elements when the smooth topology of the design model projects back to the FEA model. Therefore, it needs to calculate the volume fraction of each element for the FEA model as

$$V_i^{\mathrm{f}} = \begin{cases} 1 & \text{when } \min\left(\phi_i^j\right) > S \\ 0 & \text{when } \max(\phi_i^j) \leq S \\ N_{lp}/N_{ap} & \text{otherwise} \end{cases} \tag{25}$$

where ϕ_i^j $(j = 1, 2, \ldots)$ denotes the LSF values at nodes of element *i*. For a boundary element, $0 < V_i^{\mathrm{f}} < 1$, the element can be assumed to be divide into fine grids (40×40 in this paper) with the total N_{ap} points. N_{lp} denotes the total number of points whose LSF value is large than the level-set, S. Thus, the volume of the design model, *V*, can be calculated by the elemental volume fractions of the FEA model according to Eqn. (3). At each iteration, an appropriate value S can be easily found by setting $V = V_l$.

2.5 Convergence criterion

The optimization procedure will iteratively conduct FEA and the update of topology until the volume constraint (V^*) is reached and the following convergence criterion is satisfied.

$$\frac{\left|\left(\sum_{q=1}^{Q}\left(obj_{l-q+1} - obj_{l-Q-q+1}\right)\right)\right|}{\sum_{q=1}^{Q} obj_{l-q+1}} \leq \tau \tag{23}$$

here, *obj* denotes the objective function, e.g. *C* or ω_j. l is the current iteration number, Q is the integral number and set to be 5 in this paper, and τ is a specified small value. The convergence criterion defined in Eqn. (23) means that the value of the objective function in 10 successive iterations almost keep to be the constant. In the traditional element-based BESO method, τ = 0.1% is normally used. Since the proposed ETO method identifies the topology far beyond elements, a more strict convergence criterion τ = 0.01% is used in the paper.

3. ETO procedure

The optimization iteration of the proposed ETO method is briefly summarized as following:

1. Discretize the design domain using FE mesh for given boundary and loading conditions. Assign the initial property values of elements to construct initial design;
2. Perform fixed-grid FEA and calculate elemental sensitivity numbers;
3. Convert the elemental sensitivity numbers into nodal sensitivity numbers by the filter and average with their history information;
4. Determine the target volume for the next iteration and construct LSF;
5. Calculate elemental volume fraction of the FEA model and update the topology of the design model by the level-set value, *S*;

6. Go back to Step 2 until the volume constraint and the convergence criterion solution are satisfied;
7. Output results.

The above ETO procedure is similar to that of the BESO method but it does not involve the removal/addition of elements, which is the most important feature of the BESO method. That is why we term it with a new name, ETO rather than BESO.

4. Numerical examples

4.1 Minimum compliance for a cantilever beam

The first example considers the stiffness maximization design of a cantilever beam under a concentrated loading as shown in Fig. 4. The design domain has length 60 mm, height 40 mm and thickness 1 mm, where the force is applied downward at the center of the free end with the magnitude of 1 N. The material has Young's modulus of 1 MPa and Poisson's ration of 0.3. It is assumed that the available material can only cover 50% volume of the design domain. In order to demonstrate the advantage of the presented ETO method, a coarse mesh of size 30×20 is used to subdivide the design structure. The ETO parameters are $ER = 2\%$ and $r_{min} = 2$. The final topology is shown in Fig. 5 (a) with the structural compliance 31.35 N mm.

The above problem using the same meshes is solved using the ESO-type method given in [36] with same design parameters. The final topology is shown in Fig. 5 (b) which is similar to the above ETO topology in Fig. 5 (a) but has serrated boundaries. The compliance is 32.59 N mm which is higher than that of the ETO method. The above problem is also solved by the continuous density-based SIMP method with penalty factor $p = 3$, filter radius $r_{min} = 1.5$ and sensitivity filtering. The final topology is shown in Fig. 5 (c) which is similar with above two results except there exit "grey" elements which denote intermediate density material. The compliance is 36.77 N mm which is also higher than 31.35 N mm of the ETO topology. This may be attributed to the over-estimated strain energy of the intermediate density elements in the SIMP topology.

Fig. 6(a) shows the evolution histories of the compliance and the volume fraction. The compliance increases as the material volume fraction gradually decreases. After the volume reaches the objective volume, the compliance is convergent to an almost

constant value. The evolution history of structural topology is shown Fig. 7. As can be observed, there is barely topology change but boundary moving after about 30 iterations, and the structure finally converges to Fig. 7(f) after another 18 iterations.

To further verify the developed ETO method, it is necessary to numerically investigate the effect of the mesh refinement of the considered structure. Here, different refined meshes 90×60, 150×100 and 210×140 are assigned for the cantilever. The resulting topologies are displayed in Fig. 8 (b), (c), (d), respectively. There is no visible difference as compared to Fig. 7(f), which indicates that the mesh refinement of the structure has negligible effect on designs.

4.2 Minimum compliance for a MBB beam

In the second example, we consider the design problem for the MBB beam sketched in Fig. 9. The simple supported beam is loaded at its up center by $F = -1$ N. The symmetric right half with the dimensions $100\,mm \times 40\,mm$ is discretized into 50×20, 100×40 and 200×80 four-node quadrilateral element meshes, with the filter radii set to 3, 6, and 12, respectively. Suppose only 50% of the design domain volume material is available for constructing the final structure and the material Young's modulus is set to $E = 1\,MPa$ and the Poisson's ratio is set to $\nu = 0.3$. ER is also set to 2%. Initially, the material is full of the design domain. The optimal topologies are shown in Fig. 10, in which all meshes converge to the same optimal topology in terms of number of internal structural members, which further validates that the proposed method is capable of providing mesh-independent designs. The evolution histories of the compliance and the volume fraction of the MBB design using coarse mesh is given in Fig. 11. It is noted that apparent bumps in the compliance are caused due to significant topology variations. Thereafter, the compliance is recovered and assures that the topology develops in the right direction. The evolution history of topology is shown in Fig. 12.

4.3 Minimum compliance for a roller-supported half-wheel

The above examples show that the ETO method is able to find the optimal topology from the full material design. In this section, we conduct ETO starting from initial guess designs whose volumes are close or equal to the objective volume. The most advantage of this procedure is that only a portion of elements in the design domain

is involved in the analysis and therefore the computation time can be saved especially for finely discretized models. In order to clarify this procedure, we solve the roller-supported half-wheel design using full material design and two initial guess designs as shown in Fig. 13. The structure is loaded at its bottom center by $F = -1$ N. Material Young's modulus and Poisson's ratio are set to $E = 1\ MPa$ $\nu = 0.3$, respectively. ETO optimization parameters are set to $ER = 0.02$, and $r_{min} = 3$. Final topologies obtained from different initial designs are presented in Fig. 14, which indicates that their topologies and structural compliances are very close to each other. These calculations show that the present ETO method leads to a convergent design solution even for largely different initial guess designs. Fig. 15 shows the evolution histories of the compliances and the volume fraction when ETO starting two initial guess designs. It can be seen that the objective function decreases with the redistribution of the 50% materials. The optimization algorithm is convergent after 60 and 101 design iterations for initial guesses 1 and 2, respectively.

4.4 Design of 2D structural natural frequency

We seek the topological design that maximizes the fundamental frequency subject to a volume fraction constraint of 50% of a clamped beam in this example. Design dimensions of the beam is $140\text{mm} \times 20\text{mm}$ which is clamped on both sides as shown in Fig. 16 (a). Young's modulus $E = 1N/mm^2$, Poisson's ration $\nu = 0.3$ and mass density $\rho = 10^{-9}kg/mm^3$ are assumed. A concentrate nonstructural mass $M = 1 \times 10^{-3}kg$ is placed at the center. The rectangular design is divided into 140×20 four node plane stress elements. The ETO parameters are set to $ER = 0.02$, and $r_{min} = 2$. The optimal design obtained using the ETO method is shown in Fig. 16(b). The optimization iteration converges after 61 design iterations and the fundamental frequency of the resultant topology is $\omega_1 = 21.75\ rad/s$. Fig. 17 shows the evolution histories of the fundamental frequency as well as the volume fraction. It is seen that the volume fraction reaches its constraint value 50% after about 35 design iterations and the first natural frequency converges to a constant value after another 26 design iterations. This is because we set a very strict stop criterion to ensure the structural topological convergence.

4.5 Design of 3D structural compliance

The present ETO method can be straightforwardly extended to the 3D case. Fig. 18(a) shows support and loading conditions of a 3D cantilever beam with $F = -1$ N. Young's modulus $E = 1MPa$, and Poisson's ration $\nu = 0.3$ are assumed. The objective volume is only 50% volume of the design domain. The cubic design is divided into $60 \times 20 \times 4$ eight node brick elements. ETO parameters are $ER = 0.02$, and $r_{min} = 3$. The final topology satisfies the volume constraint and the convergence criterion is illustrated in Fig. 18(b) with smooth boundaries. The objective function converges to 23.25 N mm after only 63 iterations to satisfy the strict convergence criterion $\tau = 0.01\%$. Fig. 19 shows the evolution histories of the compliance and volume fraction.

4.6 Design of 3D structural natural frequency

It should be noted that the most time-consuming part of the optimization process is for solving the equilibrium equations in the FE analysis. Thus the computational efficiency is of critical importance for large optimization problems, especially for 3D structures. To further demonstrate the efficiency of the present ETO method, we consider a 3D structural frequency design starting from an initial guess design. The 3D design dimensions of the beam is $60 \times 10 \times 10$ which is clamped on both sides as shown in Fig. 20(a). A concentrate nonstructural mass $M = 1 \times 10^{-3}kg$ is attached to the center of the bottom surface. Young's modulus $E = 1N/mm^2$, Poisson's ration $\nu = 0.3$ and mass density $\rho = 10^{-9}kg/mm^3$ are assumed. The objective volume is 30% of the design domain and the initial guess design with 3000 elements which is less than twice the volume constraint as shown in Fig. 20(b). The ETO parameters are $ER = 0.02$, and $r_{min} = 1.5$. The topology is developed by gradually relocating solid elements following the ETO procedure outlined in Section 3 until the objective volume is reached. The optimal designs from the initial guess design is given in Fig. 20(c). The total iteration numbers and the final fundamental frequency is 95 and $312.58rad/s$, respectively. Fig. 21 shows the evolution histories of the fundamental frequency and

the volume fraction when ETO starting the initial guess design. In this case, the total volume of the model decreases step by step until the objective volume is reached. Then the volume is unchanged and the natural frequency increases gradually until the convergence criterion is satisfied. Therefore, the proposed method may start from guess designs that are much small than the full design domain. This is of important for optimizing 3D structures where the FEA takes up a large portion of the computational time of optimization.

5. Conclusion and discussion

This paper has presented an evolutionary topology optimization (ETO) method for topology optimization of continuum structures. A nodal sensitivity-based level-set function (LSF) is introduced to represent the structural topology implicitly with smooth boundary representation. The structural topology is iteratively tailored by updating the constructed LSF and the level-set value, which are also used for the calculation of elemental volume fractions at each design iteration. The new approach is demonstrated on compliance minimization problems and natural frequency maximization problems of 2D and 3D continuum structures. In contrast to conventional density-based topology optimization methods, the newly proposed ETO method achieves optimized topologies with smooth boundary representation, even when a coarse mesh is employed for FEA. The introduction of LSF and the level-set value results in the fine resolution of topology far beyond elements, thus contributing to the stable convergence of the solution. Numerical examples show that the developed ETO method is capable of generating convergent and mesh-independent solutions with smooth boundary representation, meanwhile the resultant designs are less dependent on the initial guess topology.

Acknowledgements

This work was supported by State Key Program of National Natural Science of China (61232014) and Australian Research Council (FT130101094). The first author is partially supported by the scholarship (201606130105) provided by China Scholarship Council (CSC).

Appendix

This appendix contains an ETO Matlab code for benchmark designs of structures from full material of the design domain. The code is developed on top of the 88-line code [23] with the implementation of the ETO method. The design domain is assumed rectangular and discretized into square plane stress elements. The main program is called form the Matlab prompt by the commands

eto(nelx, nely, volfrac, er, rmin, ctp)

where *nelx* and *nely* denote the total number of elements in the horizontal and vertical directions respectively, *volfrac* is the prescribed volume fraction, *er* is the evolutionary rate, *rmin* is the filter radius, and *ctp* specifies the case type of benchmark design. The *ctp* takes values 1, 2, and 3 denoting three benchmark design cases of stiffness maximization design subject to volume fraction constraint: half-MBB beam design, clamped cantilever design, and roller-supported half-wheel design.

```
function eto(nelx,nely,volfrac,er,rmin,ctp)
 %% INITIALIZATION
 vol = 1; change = 1;  ij = 0; xmin = 1e-6;
 vx = ones(nely,nelx);
 %% MATERIAL PROPERTIES
 E0 = 1; Emin = E0*xmin; nu = 0.3; pen = 3.0;
 %% PREPARE FINITE ELEMENT ANALYSIS
 A11 = [12 3 -6 -3; 3 12 3 0; -6 3 12 -3; -3 0 -3 12];
 A12 = [-6 -3 0 3; -3 -6 -3 -6; 0 -3 -6 3; 3 -6 3 -6];
 B11 = [-4 3 -2 9; 3 -4 -9 4; -2 -9 -4 -3; 9 4 -3 -4];
 B12 = [ 2 -3 4 -9; -3 2 9 -2; 4 9 2 3; -9 -2 3 2];
 KE = 1/(1-nu^2)/24*([A11 A12;A12' A11]+nu*[B11 B12;B12' B11]);
 nodenrs = reshape(1:(1+nelx)*(1+nely),1+nely,1+ nelx);
 edofVec = reshape(2*nodenrs(1:end-1,1:end-1)+1,nelx*nely,1);
 edofMat = repmat(edofVec,1,8)+repmat([0 1 2*nely+[2 3 0 1] -2 -
1],nelx*nely,1);
 iK = reshape(kron(edofMat,ones(8,1))',64*nelx*nely,1);
 jK = reshape(kron(edofMat,ones(1,8))',64*nelx*nely,1);
 %% ELEMENTAL NODES AND COORDINATES
 nodelast = reshape(nodenrs(1:end-1,1:end-1),nelx*nely,1);
 elenod = repmat(nodelast,1,4)+repmat([1 nely+[2 1] 0 ],nelx*nely,1);
 [nodex,nodey] = meshgrid(0:1:nelx,nely:-1:0);
 %% DEFINE LOADS AND SUPPORTS
switch(ctp)
```

```
 case 1 % HALF-MBB BEAM
 F = sparse(2,1,-1,2*(nely+1)*(nelx+1),1);
 fixeddofs = union(1:2:2*(nely+1), 2*(nely+1)*(nelx+1));
 case 2 % CANTILEVER
 F = sparse(2*(nely+1)*(nelx+1)-nely,1,-1,2*(nely+1)*(nelx+1),1);
 fixeddofs = (1:2*(nely+1));
 case 3 % HALF-WHEEL
 F = sparse(2*(nely+1)*(nelx/2+1),1,-1,2*(nely+1)*(nelx+1),1);
 fixeddofs = union(2*nely+1:2*(nely+1), 2*(nely+1)*(nelx+1));
 end
 U = zeros(2*(nely+1)*(nelx+1),1);
 alldofs = (1:2*(nely+1)*(nelx+1));
 freedofs = setdiff(alldofs,fixeddofs);
 %% PREPARE FILTER
 iH = ones((nelx+1)*(nely+1)*(2*(ceil(rmin)+1))^2,1);
 jH = ones(size(iH)); sH = zeros(size(iH)); k = 0;
 [elex,eley] = meshgrid(1.5:nelx+0.5,1.5:nely+0.5);
 for i1 = 1:nelx+1
   for j1 = 1:nely+1
       e1 = (i1-1)*(nely+1)+j1;
         for i2 = max(i1-ceil(rmin),1):min(i1+ceil(rmin)-1,nelx)
             for j2 = max(j1-ceil(rmin),1):min(j1+ceil(rmin)-1,nely)
                 e2 = (i2-1)*nely+j2; k = k+1; iH(k) = e1;
                 jH(k) = e2;
                 sH(k) = max(0,rmin-sqrt((i1-elex(j2,i2))^2+(j1-
eley(j2,i2))^2));
             end
         end
    end
 end
 H = sparse(iH,jH,sH); Hs = sum(H,2);
 %% START ITERATION
while change > 0.0001
 ij = ij + 1; vol = max(vol*(1-er), volfrac);
 if ij > 1; olddcnd = dcnd; end
 %% FE-ANALYSIS
 sK = reshape(KE(:)*(vx(:)'*E0+(1-vx(:))'*Emin),64*nelx*nely,1);
 K = sparse(iK,jK,sK); K = (K+K')/2;
 U(freedofs) = K(freedofs,freedofs)\F(freedofs);
 %% OBJECTIVE FUNCTION AND SENSITIVITY ANALYSIS
 ce = reshape(sum((U(edofMat)*KE).*U(edofMat),2),nely,nelx);
 c(ij) = sum(sum((vx.*E0+(1-vx).*Emin).*ce));
```

```
 dc = ((1-vx)*xmin.^(pen-1)+vx)*E0.*ce;
 %% FILTERING/MODIFICATION OF NODAL SENSITIVITIES
 dcnd = reshape((H*dc(:)./Hs),nely+1,nelx+1);
 if ij > 1; dcnd = (dcnd+olddcnd)/2.; end
 %% OPTIMALITY CRITERIA UPDATE OF ELEMENT VOLUME
 l1 = min(dcnd(:)); l2 = max(dcnd(:));
 while (l2-l1)/abs(l1+l2) > 1.0e-9
 ls = (l1+l2)/2.0;
 dcth = dcnd(:)-ls;
   for i = 1:nely*nelx
      if min(dcth(elenod(i,:))) > 0
         vx(i) = 1;
      elseif max(dcth(elenod(i,:))) < 0
         vx(i) = 0;
      else
         ngrid = 40; [s,t] = meshgrid(-1+1/ngrid:2/ngrid:1-1/ngrid,-
1+1/ngrid:2/ngrid:1-1/ngrid);
         ps = (1 - s(:)).*(1 - t(:))/4 * dcth(elenod(i,1)) + (1 +
s(:)).*(1 - t(:))/4 * dcth(elenod(i,2))...
            + (1 + s(:)).*(1 + t(:))/4 * dcth(elenod(i,3)) + (1-
s(:)).*(1 + t(:))/4 * dcth(elenod(i,4));
         vx(i) = length(find( ps >= 0 ))/length(s(:));
      end
   end
 if mean(vx(:)) - vol > 0;
 l1 = ls;
 else
 l2 = ls;
 end
 end
 %% PLOT RESULTS
 if ij > 10; change =abs(sum(c(ij-9:ij-5))-sum(c(ij-4:ij)))/sum(c(ij-
4:ij)); end
 fprintf('It.:%3i Obj.:%8.4f Vol.:%4.3f
ch.:%4.5f\n',(ij),c(ij),mean(vx(:)),change);
 contourf(nodex, nodey, (dcnd-ls), [0 0] ); axis equal;  axis tight;
axis off; pause(1e-6);
end
```

References

[1] M.P. Bendsøe, N. Kikuchi, Generating optimal topologies in structural design using

a homogenization method, Comput. Methods Appl. Mech. Engrg. 71 (1988) 197–224.

[2] M.P. Bendsøe, Optimal shape design as a material distribution problem, Struct. Optim. 1 (4) (1989) 193–202.

[3] M. Zhou, G.I.N. Rozvany, The coc algorithm, part ii: Topological, geometrical and generalized shape optimization, Comput. Methods Appl. Mech. Engrg. 89 (1–3) (1991) 309–336.

[4] M.P. Bendsøe, O. Sigmund, Topology Optimization: Theory, Methods and Applications, Springer-Verlag, Berlin, 2003.

[5] Y.M. Xie, G.P. Steven, A simple evolutionary procedure for structural optimization, Comput. Struct. 49 (5) (1993) 885–896.

[6] Y.M. Xie, G.P. Steven, Evolutionary Structural Optimization, Springer-Verlag, London, 1997.

[7] J.A. Sethian, A. Wiegmann, Structural boundary design via level set and immersed interface methods, J. Comput. Phys. 163 (2) (2000) 489–528.

[8] M.Y. Wang, X. Wang, D. Guo, A level set method for structural topology optimization, Comput. Methods Appl. Mech. Engrg. 192 (1–2) (2003) 227–246.

[9] G. Allaire, F. Jouve, A.M. Toader, Structural optimization using sensitivity analysis and a level-set method, J. Comput. Phys. 194 (1) (2004) 363–393.

[10] A Tovar, GL Niebur. M Sen, J Renaud, “Bone structure adaptation as a cellular automaton optimization process”. In 45th AIAA/ASME/ASCE/AHS/ASC Structures, Structural Dynamics and Materials Conference (2004) AIAA 2004-17862.

[11] B Bourdin, A. Chambolle, Design-dependent loads in topology optimization. ESAIM - Control Optim and Cal of Var (9) (2003):19–48

[12] J.D. Deaton, R.V. Grandhi, A survey of structural and multi-disciplinary continuum topology optimization: post 2000. Struct. Multidiscip. Optim. 49(1) (2014) 1–38

[13] O. Sigmund, K. Maute, Topology optimization approaches — a comparative review, Struct. Multidiscip. Optim. 48 (6) (2013) 1031–1055.

[14] MY. Wang, X. Wang, “Color” level sets: a multi-phase method for structural topology optimization with multiple materials. Comput Methods Appl Mech Eng 193(6–8) (2004) 469–496

[15] K.S. Park, S.K. Youn, Topology optimization of shell structures using adaptive

inner-front (AIF) level set method. Struct Multidisc Optim 36 (1) (2008) 43-58

[16] Z. Luo, L. Tong, A level set method for shape and topology optimization of large-displacement compliant mechanisms. Int J Numer Methods Eng 76(6) (2008)862–892

[17] G. Allaire, F. Jouve, Minimum stress optimal design with the level set method. Eng Anal Bound Elem 32(11) (2008) 909–918

[18] A. Myśliński, Level set method for optimization of contact problems. Eng Anal Bound Elem 32(11) (2008)986–994

[19] N. Van Dijk, K. Maute, M. Langelaar, F. van Keulen, Level-set methods for structural topology optimization: A review, Struct. Multidiscip. Optim.48(3) (2013) 437–472

[20] H.P. Mlejnek, Some aspects of the genesis of structures, Struct. Multidiscip. Optim. 5 (1992) 64-69

[21] M.P. Bendsøe, O. Sigmund, Material interpolations in topology optimization, Arch. Appl. Mech, 69 (1999) 635-654

[22] O. Sigmund, A 99 line topology optimization code written in Matlab, Struct. Multidiscip. Optim. 21 (1999) 120-127.

[23] E. Andreassen, A Clausen, M Schevenels, B. S. Lazarov, O. Sigmund, Efficient topology optimization in MATLAB using 88 lines of code, Struct. Multidiscip. Optim. 43 (2011) 1-16.

[24] P. Tanskanen, The evolutionary structural optimization method: Theoretical aspects. Comput. Methods Appl. Mech. Engrg. 191(47-48) (2002)5485–5498.

[25] X. Huang, Y.M. Xie, Convergent and mesh-independent solutions for the bi-directional evolutionary structural optimization method. Finite. Elem. Anal. Des. 43(14) (2007) 1039–1049.

[26] X. Huang, Y.M. Xie, Topology optimization of nonlinear structures under displacement loading, Eng. Struct. 30(7) (2008)2057–2068.

[27] X. Huang, Z. Zuo, Y.M. Xie, Evolutionary topological optimization of vibrating continuum structures for natural frequencies. Comput. Struct. 88(5) (2010) 357–364

[28] X. Huang, A. Radman, Y.M. Xie, Topological design of microstructures of cellular materials for maximum bulk or shear modulus. Comput. Mater. Sci. 50(6) (2011) 1861–1870.

[29] L. Xia, P. Breitkopf, Concurrent topology optimization design of material and

structure within fe^2 nonlinear multiscale analysis framework. Comput. Methods Appl. Mech. Engrg. 278 (2014) 524–542.

[30] L. Xia, P. Breitkopf, A reduced multiscale model for nonlinear structural topology optimization. Comput. Methods Appl. Mech. Engrg. 280 (2014)117–134.

[31] X. Huang, S. Zhou, G. Sun, G. Li, Y.M. Xie, Topology optimization for microstructures of viscoelastic composite materials, Comput. Methods Appl. Mech. Engrg. 283 (2015) 503–516.

[32] L. Xia, P. Breitkopf, Multiscale structural topology optimization with an approximate constitutive model for local material microstructure. Comput. Methods Appl. Mech. Engrg. 286 (2015) 147–167.

[33] D.C. Da, X.Y. Cui, K. Long, G.Y. Li, Concurrent topological design of composite structures and the underlying multi-phase materials, Comput. Struct. 179 (2017) 1–14.

[34] W.M. Vicente, R. Picelli, R. Pavanello, Y.M. Xie, Topology optimization of frequency responses of fluid-structure interaction systems, Finite Elem Anal Des 98 (2015) 1-13.

[35] Y.M. Xie, G.P. Steven, Evolutionary Structural Optimization. Springer-Verlag, London, 1997.

[36] X. Huang, Y.M. Xie, Topology Optimization of Continuum Structures: Methods and Applications. John Wiley & Sons, Chichester, 2010.

[37] L. Xia, Q. Xia, X. Huang, Y.M. Xie, Bi-directional evolutionary structural optimization on advanced structures and materials: a comprehensive review, Arch Comput Methods Eng, (2016) DOI: 10.1007/s11831-016-9203-2.

[38] J.A. Sethian, A. Wiegmann, Structural boundary design via level set and immersed interface methods, J. Comp. Phys. 163 (2000) 489-528.

[39] M.J. Garcia, G.P. Steven, Fixed grid finite elements in elasticity problems, Eng Computation 16 (2) (1999) 145-164.

[40] H. Kim, M.J. Garcia, O.M. Querin, G.P. Steven and Y.M. Xie, Introduction of fixed grid in evolutionary structural optimization. Engineering Computation, 17 (2000) 427-439.

[41] M. J. García, O. E. Ruíz, G. P. Steven, Engineering design using evolutionary structural optimisation based on iso-stress-driven smooth geometry removal. NAFEMS world congress. 2001.

[42] Y. Liu, F. Jin, Q. Li, S. Zhou, A fixed-grid bidirectional evolutionary structural optimization method and its applications in tunneling engineering, Inter. J. Num. Meth. Eng. 73 (2008) 1788-1710.

[43] S.Y. Wang, K.M. Lim, B.C. Khoo, M.Y. Wang, An extended level set method for shape and topology optimization. J. Comp. Phys. 221 (2007) 395-421.

[44] S. Lee, B.M. Kawak, Smooth boundary topology optimization for eigenvalue performance and its application to the design of a flexural stage. Eng. Optim. 40 (2008) 271-285.

[45] J. Luo, Z. Luo, L.Chen, L. Tong, M.Y. Wang, A semi-implicit level set method for structural shape and topology optimization. J. Comp. Phys. 227 (2008) 5561-5581.

[46] H.P. Jia, H.G. Beom, Y.X. Wang, S. Lin, B. Liu, Evolutionary level set method for structural topology optimization, Comput. Struct. 89 (2011) 445-454.

[47] NL Pedersen. Maximization of eigenvalues using topology optimization. Struct. Multidiscip. Optimiz. 20 (2000) 2–11.

[48] J.K. Guest, J.H. Prévost and T. Belytschko, Achieving minimum length scale in topology optimization using nodal design variables and projection functions. Inter. J. Numer. Methods Eng. 61 (2004) 238-254.

[49] O. Sigmund and J. Petersson, Numerical instabilities in topology optimization: A survey on procedures dealing with checkerboards, mesh-dependencies and local minima. Strct. Optim. 16 (1998) 68-75.

(a) Figures

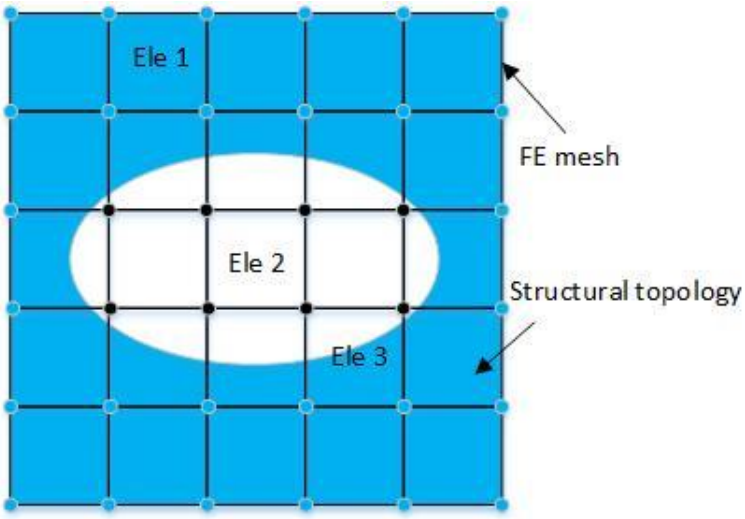

(a) Design model(structural topology) and the projected background mesh (FEA)

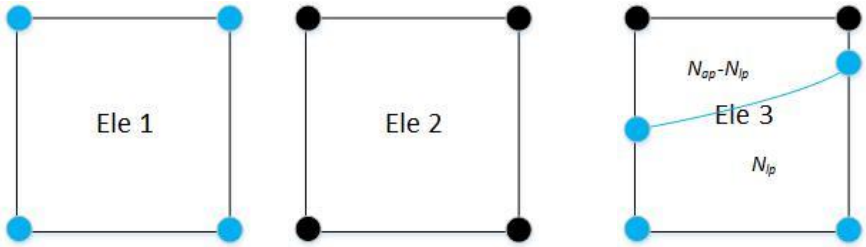

(b) Element 1 ($V_1^{\mathrm{f}} = 1$) (c) Element 2 (void) (d) Element 3 ($V_3^{\mathrm{f}} = N_{lp}/N_{ap}$)

Fig. 1. Design model (structural topology) and the projected background mesh (FEA) result three categories of elements.

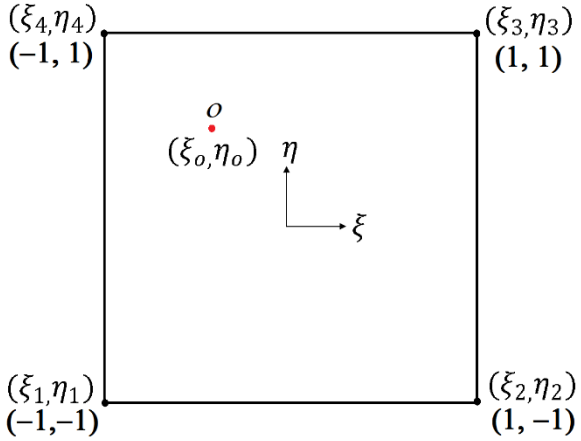

Fig. 2. An arbitrary point, $o(\xi_o, \eta_o)$, within an rectangular element under the natural coordinate system.

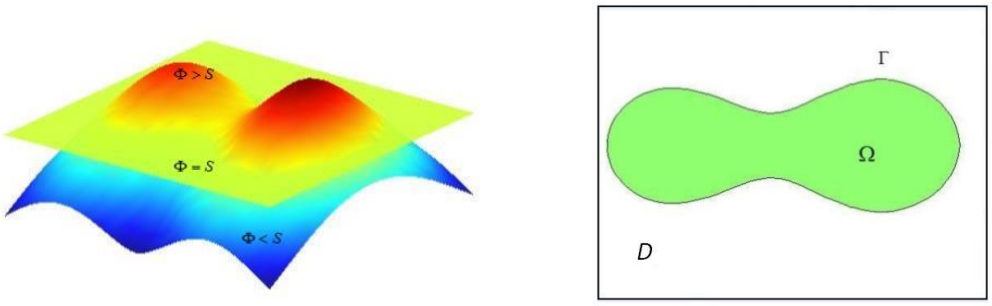

(a) (b)

Fig . 3. Illustration of LSF, level-set value and the corresponding structural topology for a 2D case (a) LSF and level-set value; (b) solid region, Ω, void regions, D/Ω and structural boundary, Γ.

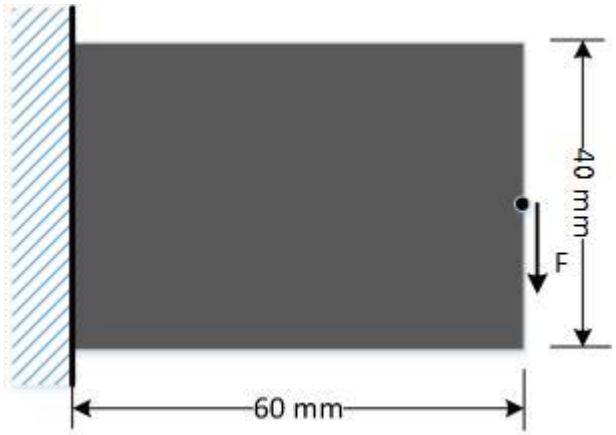

Fig. 4. Dimensions of the design domain and boundary and loading conditions of a cantilever beam.

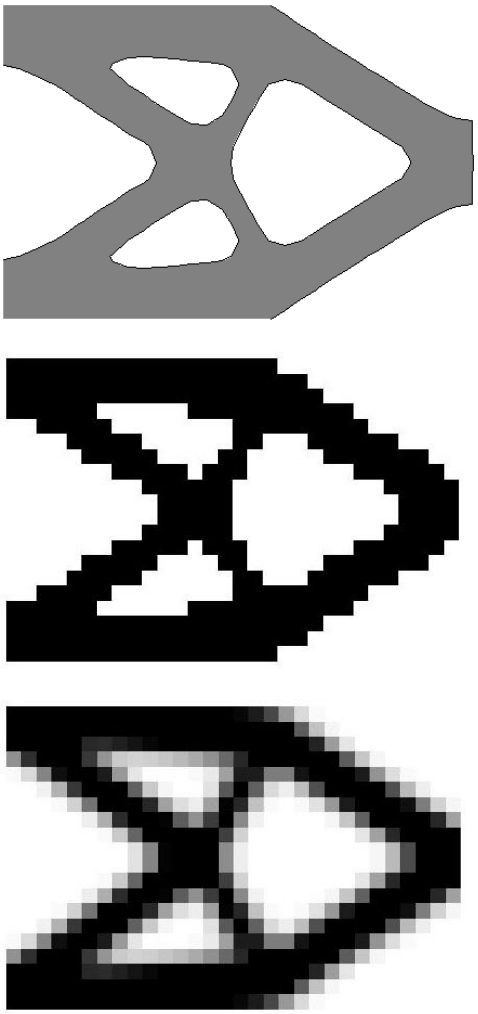

Fig. 5. Final topologies and structural compliance of the cantilever beam using different methods with same coarse mesh.

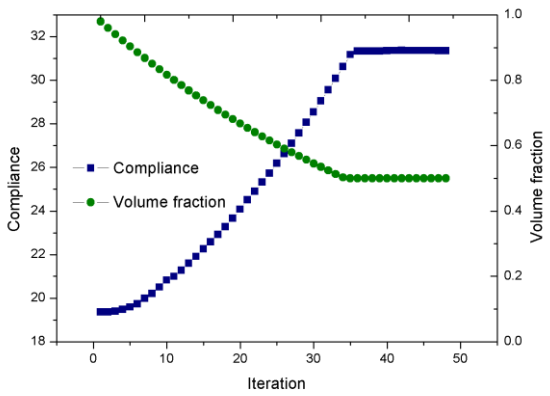

Fig. 6. Evolutionary histories of the compliance and the volume fraction for the cantilever beam.

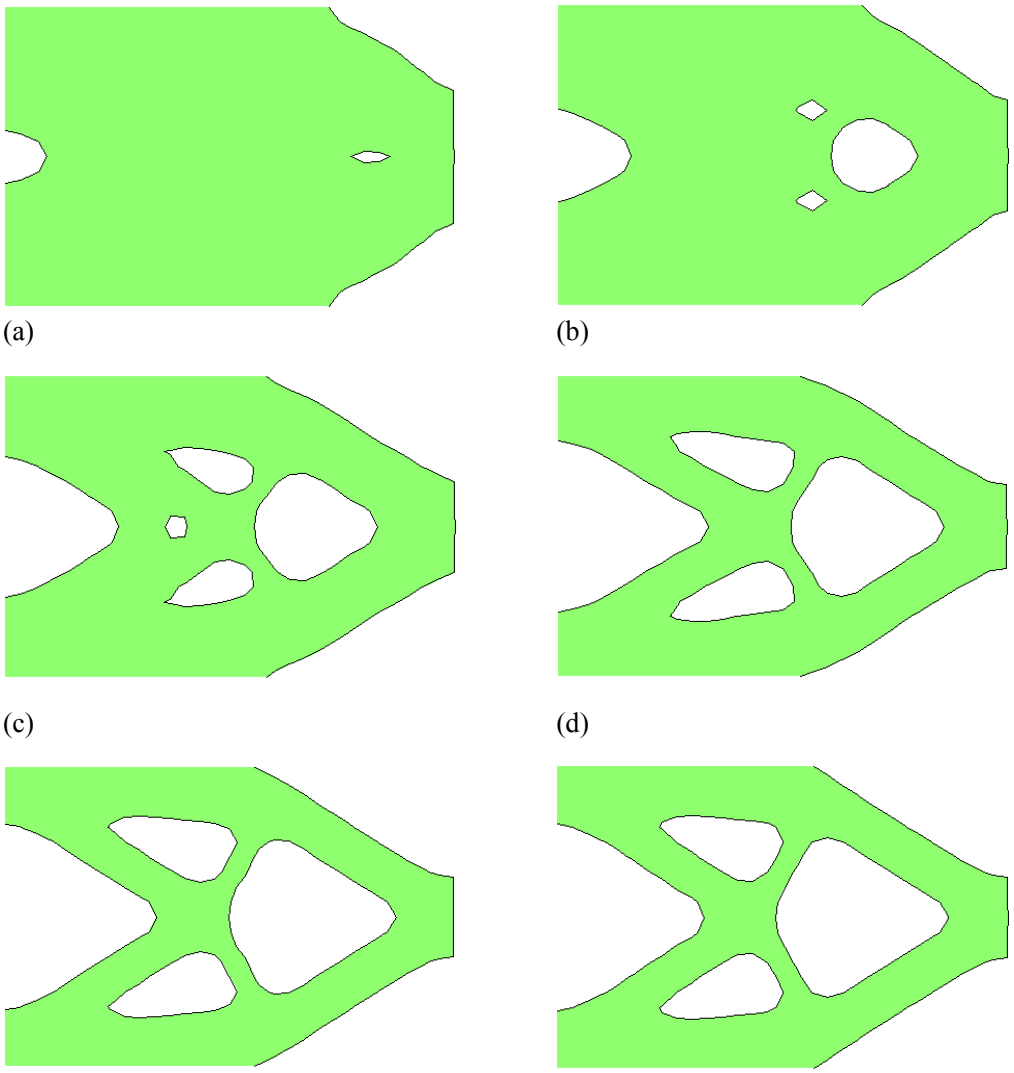

Fig. 7. Evolution of the topology: (a) iteration 5, and (b) iteration 10, and (c) iteration 20, and (d) iteration 30, and (e) iteration 40, and (f) final topology.

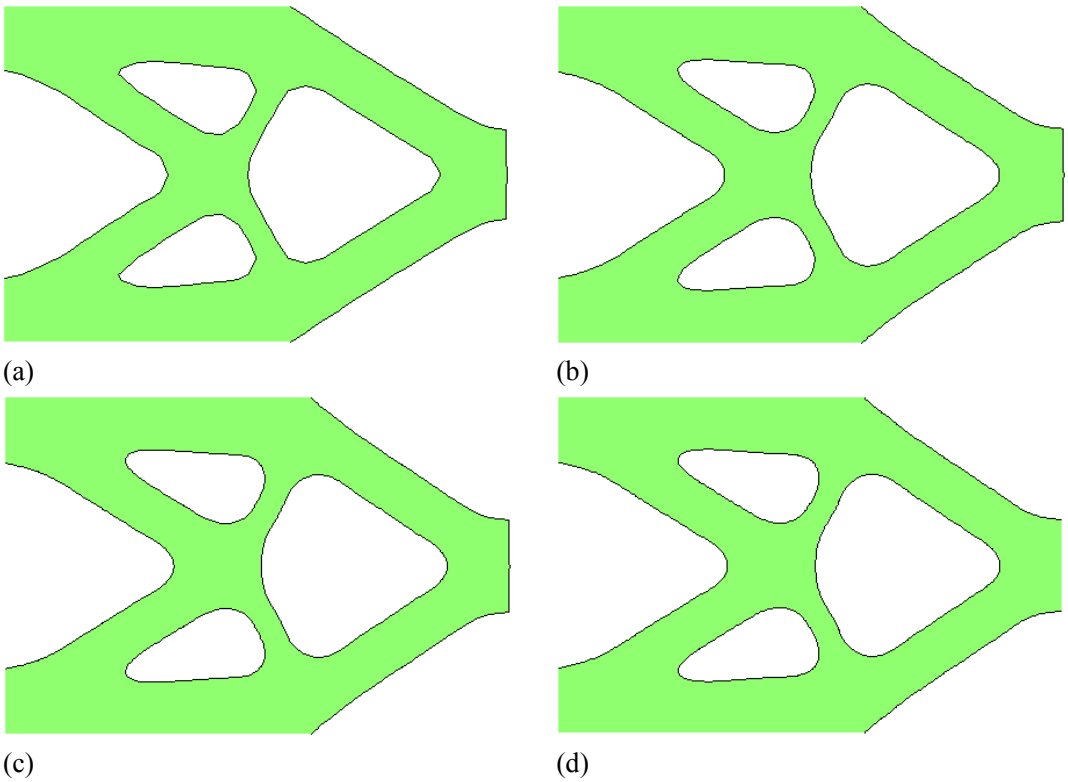

Fig. 8. Mesh-independent solutions of the cantilever: (a) 30×20, (b) 90×60, (c) 150×100, (d) 210×140.

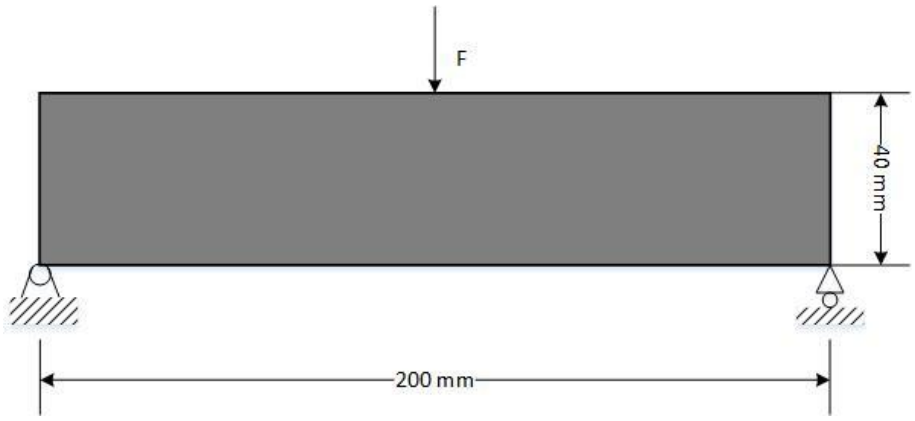

Fig. 9. Dimensions of the design domain and boundary and loading conditions of a MBB beam.

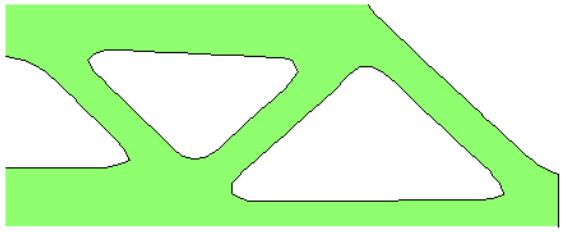

(a) Coarse mesh

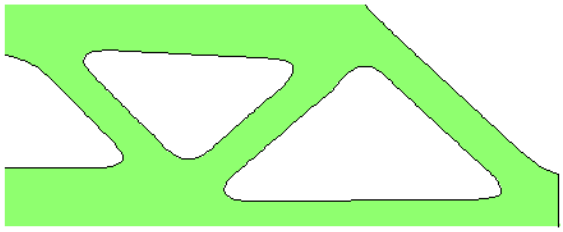

(b) Regular mesh

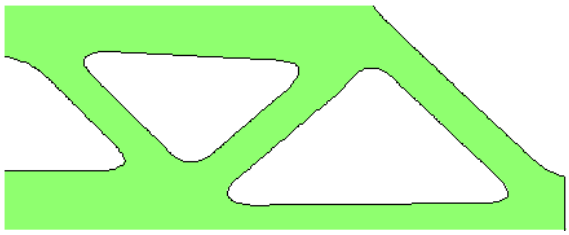

(c) Fine mesh

Fig. 10. Mesh-independent solutions of the MBB beam: (a) 50×20; (b) 100×40; (c) 200×80.

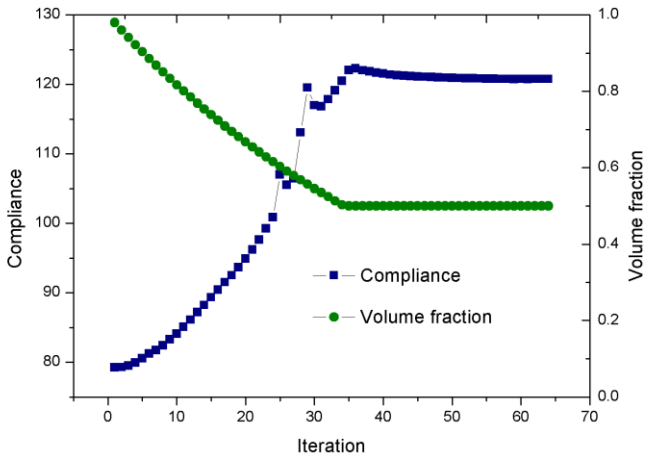

Fig .11. Evolutionary histories of the compliance and the volume fraction of the MBB beam.

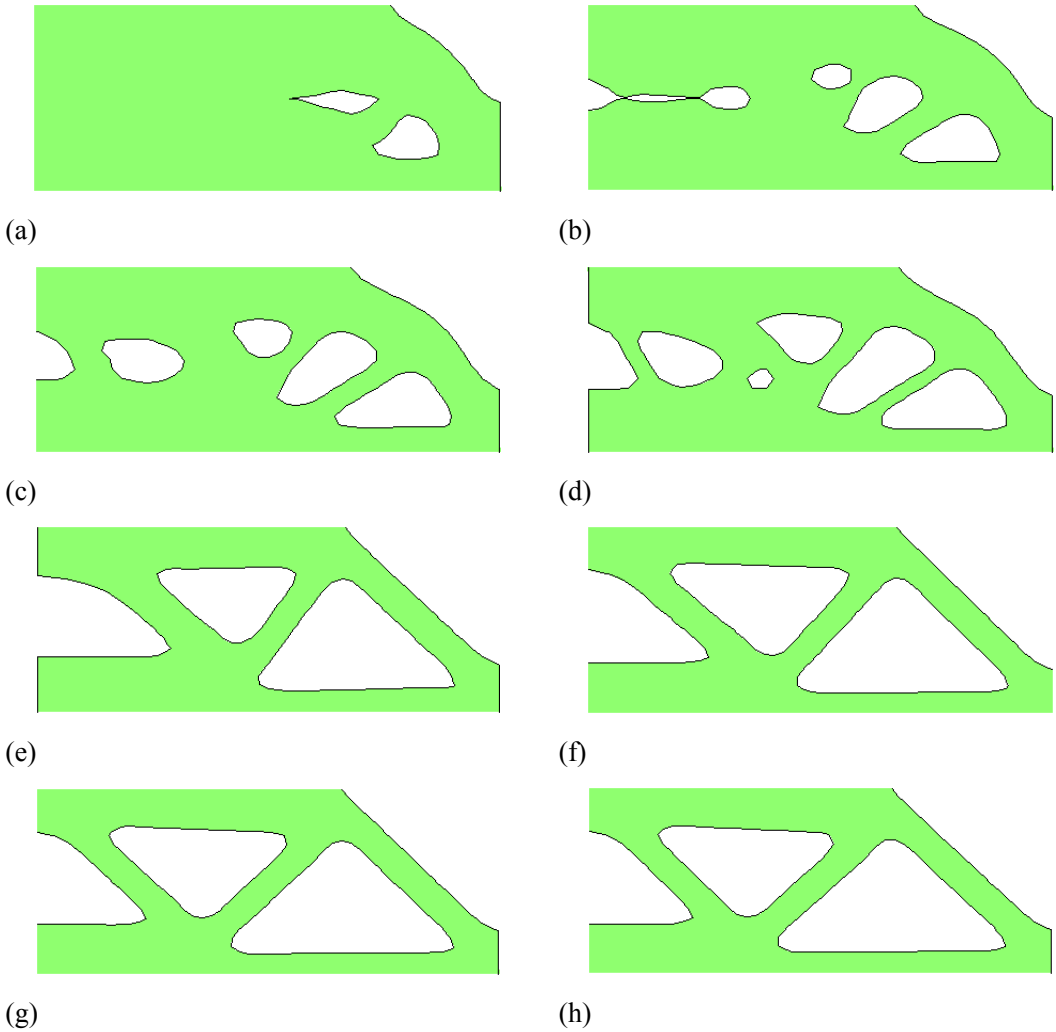

Fig. 12. Evolution of topology: (a) iteration 5, and (b) iteration 10, and (c) iteration 15, and (d) iteration 20, and (e) iteration 30, and (f) iteration 40, and (g) iteration 50, and (h) final topology.

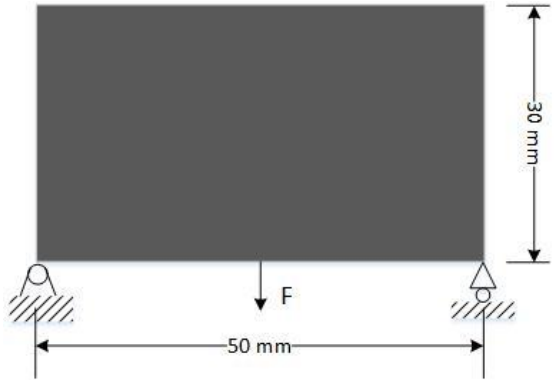

(a) Full material design

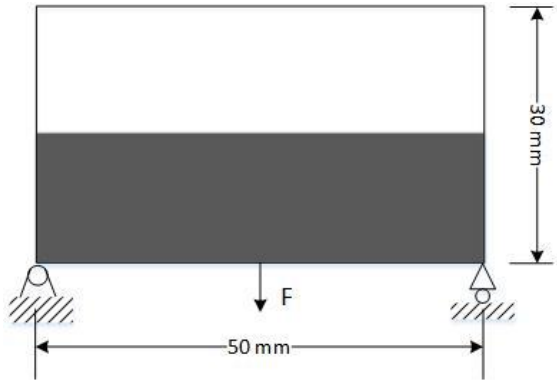

(b) Initial guess design 1

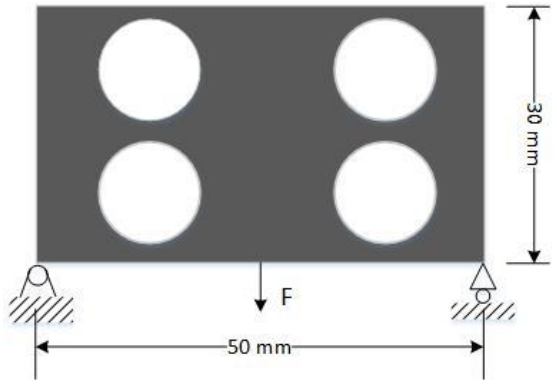

(c) Initial guess design 2

Fig. 13. Dimensions of the design domain and boundary conditions of a roller-supported half-wheel with different initial guess designs

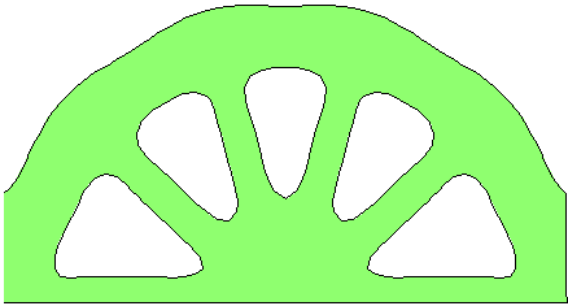

(b) Final topology from full material design: $C = 11.33$

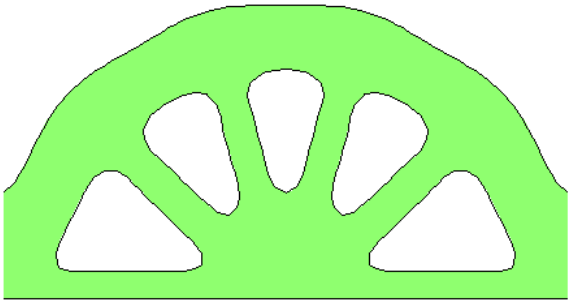

(c) Final topology from initial guess design 1: $C = 11.35$

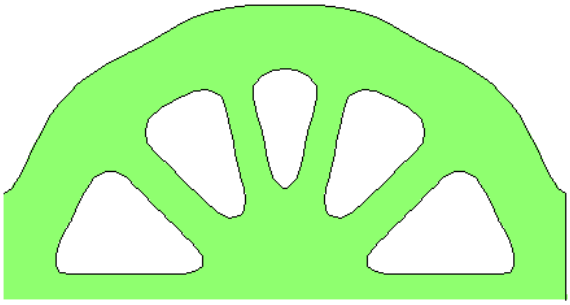

(d) Final topology from initial guess design 2: $C = 11.34$

Fig. 14. Final topologies from three different initial designs.

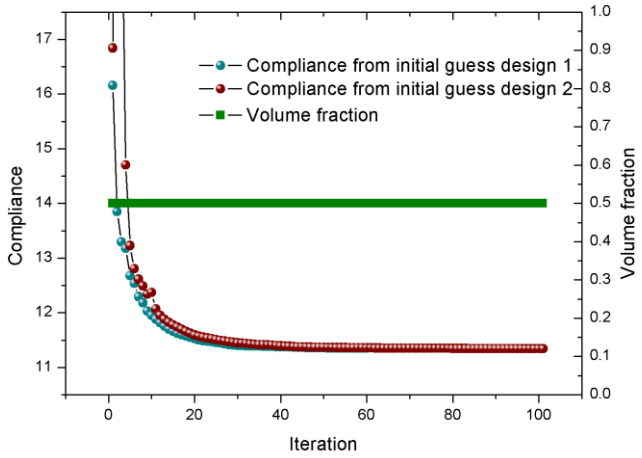

Fig. 15. Evolutionary histories of the compliances and the volume fraction when ETO starts from two initial guess designs.

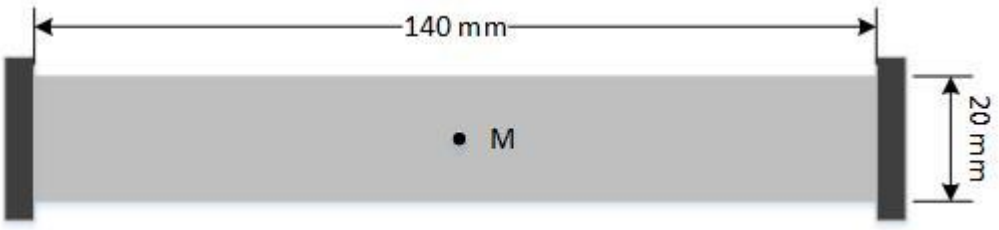

(a) design domain and boundary conditions of frequency optimization

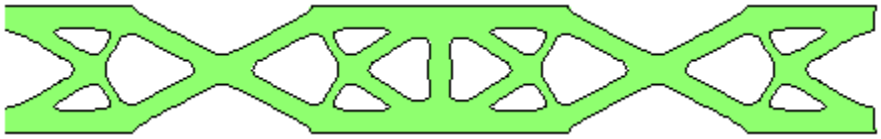

(b) solution

Fig. 16. ETO design of a clamped beam with a concentrated mass.

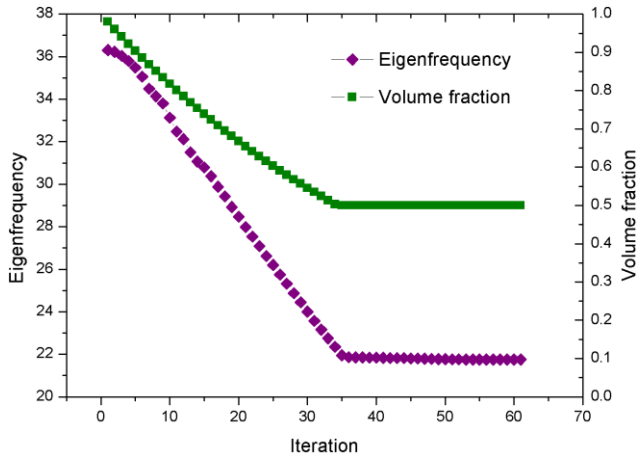

Fig. 17. Evolutionary histories of the first natural frequency and the volume fraction.

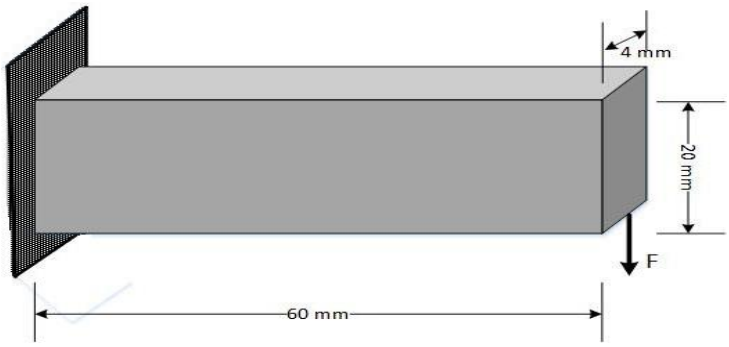

(a) design domain and boundary conditions of a cantilever beam

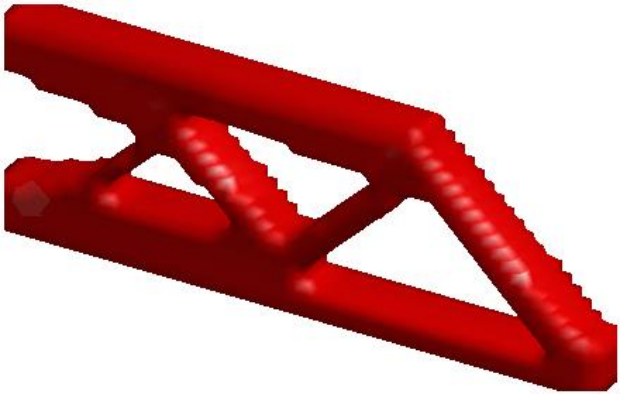

(b) Solution

Fig. 18. ETO design of a 3D cantilever beam with a concentrated force.

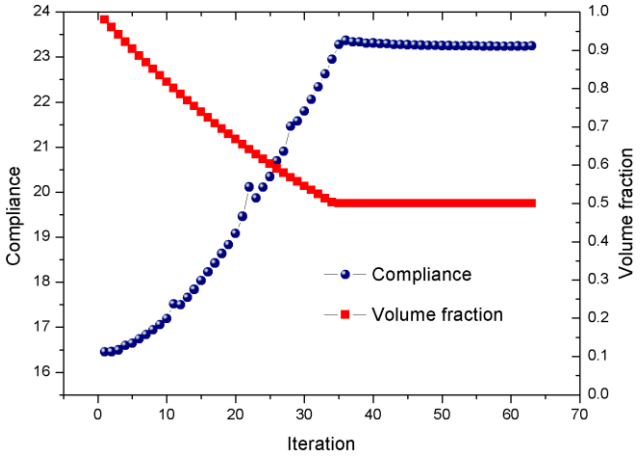

Fig .19. Evolutionary histories of the compliance and the volume fraction of the 3D cantilever beam.

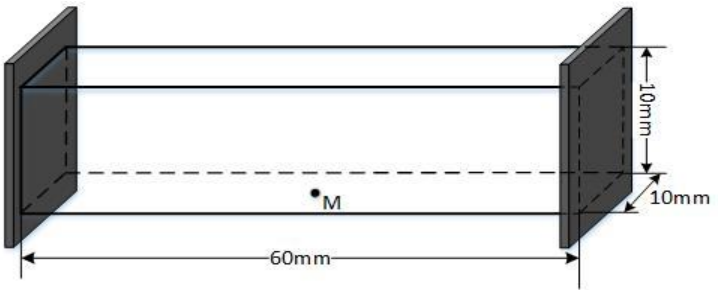

(a) design domain and boundary conditions of frequency optimization

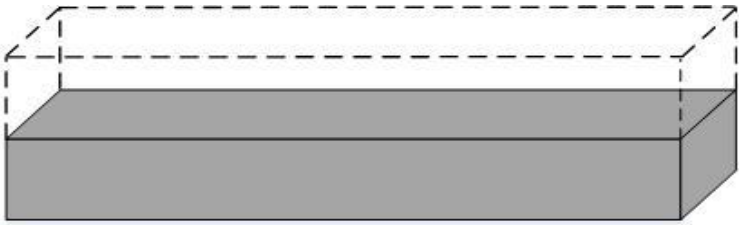

(b) initial gauss design

(c) solution

Fig. 20. ETO design of a 3D beam with a concentrated mass.

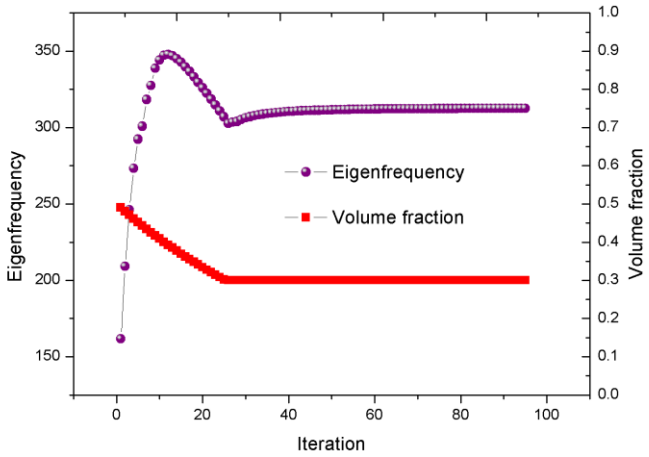

Fig. 21. Evolutionary histories of the first natural frequency and the volume fraction when ETO starts from the initial guess design.